ISSN 1063-7834, Physics of the Solid State, 2018, Vol. 60, No. 8, pp. 1514–1526. © Pleiades Publishing, Ltd., 2018.
Original Russian Text © E.L. Ivchenko, 2018, published in Fizika Tverdogo Tela, 2018, Vol. 60, No. 8, pp. 1503–1514.

SEMICONDUCTORS

Magnetic Circular Polarization of Exciton Photoluminescence

E. L. Ivchenko

Ioffe Institute, St. Petersburg, 194021 Russia
e-mail: ivchenko@coherent.ioffe.ru

Abstract—Experimental and theoretical studies of circular polarization of photoluminescence of excitons (MCPL) in semiconductors placed in an external magnetic field are reviewed. The advantage of the MCPL method is its relative simplicity. In particular, it does not require spectral resolution of the Zeeman sublevels of an exciton and may be applied to a wide class of objects having broad photoluminescence spectral lines or bands: in bulk semiconductors with excitons localized on the defects of the crystal lattice and composition fluctuations, in structures with quantum wells and quantum dots of types I and II, in two-dimensional transition metals dichalcogenides and quantum microcavities. The basic mechanisms of the magnetic circular polarization of luminescence are considered. It is shown that either known mechanisms should be modified or additional mechanisms of the MCPL should be developed to describe the polarized photoluminescence in newly invented nanosystems.

DOI: 10.1134/S1063783418080127

1. INTRODUCTION

Soon after performing his pioneering works on excitons, Ya.I. Frenkel predicted that excitons of two types may exist in a crystal, and he called them "free" and "bound" [1]. In the case of the second type exciton, a local deformation of the lattice appears, which may lower significantly the group velocity of propagation of an electron excitation and even immobilize the excitation. The idea of two exciton types was also developed by Davydov [2] ("excitation waves of types A and B") and by Dykman and Pekar [3] ("nonpolarizing" and "polarizing" excitons); see also review [4]. It is just one step from the notion of a bound or polarizing exciton (called later self-localized [5]) to the idea of an exciton localized on a lattice defect (ionized or neutral donor or acceptor, isoelectronic trap) and other fixed exciton complexes [6–11]. Narrow photoluminescence (PL) lines of these complexes are split in the magnetic field; their fine structure can be resolved spectrally and by their polarization. In this paper, we consider bulk and low-dimensional solid-state systems in which the exciton luminescence bandwidth is much larger than the exchange and Zeeman splitting of exciton levels, due to the inhomogeneous broadening of the exciton's resonance frequency. This situation takes place when excitons are localized on deep levels in bulk crystals [12] or on composition fluctuations in solid solutions [13], on the fluctuations of the width of quantum wells [14, 15] or cross-section area of quantum wires, on the interfaces of a type II superlattice [16], and also in the case of size quantum effects found for excitons in quantum dots [17] or colloid nanocrystals [18, 19] allowing for the dispersion of their size and shape within the illuminated spot. This spectrally hidden fine structure manifests itself in the magnetic circular polarization of luminescence (MCPL) and in the dependence of the luminescence intensity on the magnetic field.

The paper is organized as follows. Changes in the energy spectrum of a localized exciton in the longitudinal magnetic field are considered in Section 2. Section 3 presents formulas for the intensity and circular polarization of photoluminescence in the simplest quasi-equilibrium model neglecting the exchange interaction; exciton sublevel anticrossing allowing for the exchange interaction is discussed; a review of experimental works on the MCPL in bulk semiconductor crystals, solid solutions and nanostructures are given. Results of recent research [20–22] on the MCPL in an ultrathin GaAs/AlAs quantum well with the type II heterojunction and an indirect band gap are presented in Section 4. Magnetoluminescence of excitons and trions in quantum wells and two-dimensional transition metals dichalcogenides is discussed in Section 5. A separate Section 6 is dedicated to the MCPL of exciton magnetic polarons in diluted magnetic semiconductors and excitons polaritons in microcavities, and to paraexcitons in cuprous oxide crystals [23], where Wannier–Mott excitons were observed for the first time [24].

2. RESULTS AND DISCUSSION

2.1. Changes in the Exciton Fine Structure in the Longitudinal Magnetic Field

Allowing for the spin of free carriers but neglecting the electron-hole exchange interaction, the ground level of an exciton is degenerate. The degenerate states form a basis of some representation D_{exc} with the dimensionality one or more of the symmetry point group F of the localizing potential. Exchange interaction partially removes the degeneracy of the exciton level, and the latter is thus split into sublevels corresponding to irreducible representations of the group F. In the longitudinal magnetic field an additional modification of the exciton spectrum occurs, in particular, the remaining degeneracy of the exciton states is removed. Each of the split, optically active states emits circularly or elliptically polarized light in the direction of the magnetic field. When these states are selectively populated, the photoluminescence acquires circular polarization. In this section we will consider two most usual types of excitons: a heavy-hole exciton (denoted briefly X_{e-hh} and a triplet exciton X_{trip}.

A. Heavy-hole exciton. Model of an exciton X_{e-hh} consisting of an electron in the conduction band having the spin $s = \pm 1/2$ and a heavy hole with the projection of the angular momentum $j = \pm 3/2$ (see review [25]) is applicable for studying radiation of localized excitons in quantum wells and quantum dots, based on A_3B_5 and A_2B_6 semiconductors, in type I and II GaAs/AlAs superlattices, and in bulk solid solutions $CdS_{1-x}Se_x$. If not stated otherwise, here we consider the geometry in which the magnetic field is oriented along the normal z to the outer sample surface, and intensity and polarization of light emitted along z is studied.

Spin Hamiltonian $\mathcal{H}_{\text{exc}} = E_0 + \mathcal{H}_{\text{exch}} + \mathcal{H}_B$ of X_{e-hh} contains the exchange interaction operator [26]

$$\mathcal{H}_{\text{exch}} = \frac{1}{2}\begin{bmatrix} \delta_0 & \delta_2 & 0 & 0 \\ \delta_2 & \delta_0 & 0 & 0 \\ 0 & 0 & -\delta_0 & \delta_1 \\ 0 & 0 & \delta_1 & -\delta_0 \end{bmatrix} \quad (1)$$

and the operator of the Zeeman interaction of the electron and hole spins with the longitudinal magnetic field

$$\mathcal{H}_B = \frac{1}{2}\mu_B B_z \times \begin{bmatrix} -g_e + g_{hh} & 0 & 0 & 0 \\ 0 & g_e - g_{hh} & 0 & 0 \\ 0 & 0 & g_e + g_{hh} & 0 \\ 0 & 0 & 0 & -g_e - g_{hh} \end{bmatrix}. \quad (2)$$

Here, E_0 is the excitation energy of a "mechanical" exciton; the matrix elements are presented on the basis of exciton states $|m\rangle$ with a given total spin projection $m = s + j = 1, -1, 2, -2$; constants δ_n ($n = 0, 1, 2$) describe the doublet–doublet splitting, the splittings of the nonradiative ("dark," $m = \pm 2$) and radiative ("light," $m = \pm 1$) doublets, respectively; μ_B is the Bohr magneton; g_e and g_{hh} are effective g factors of the electron and heavy hole. For nanostructures grown in the direction $z \parallel [001]$, the matrix elements of the optical excitation of the basis states $|m\rangle$ are written as

$$M_{\pm 1} = M_0(e_x \pm ie_y), \quad M_{\pm 2} = 0,$$

where e_x and e_y are the lateral components of the light polarization vector in the axes $x \parallel [110]$ and $y \parallel [\bar{1}10]$; M_0 is a polarization-independent coefficient. Energies of the quartet sublevels in the magnetic field are given by the expressions

$$E_{1,2} = E_0 + \frac{1}{2}(\delta_0 \pm \sqrt{\delta_2^2 + (g_e - g_{hh})^2\mu_B^2 B_z^2}),$$
$$E_{3,4} = E_0 + \frac{1}{2}(-\delta_0 \pm \sqrt{\delta_1^2 + (g_e + g_{hh})^2\mu_B^2 B_z^2}). \quad (3)$$

The dependence of these sublevel energies on the magnetic field is schematically drawn in Fig. 1a; splittings δ_n are also shown in the figure.

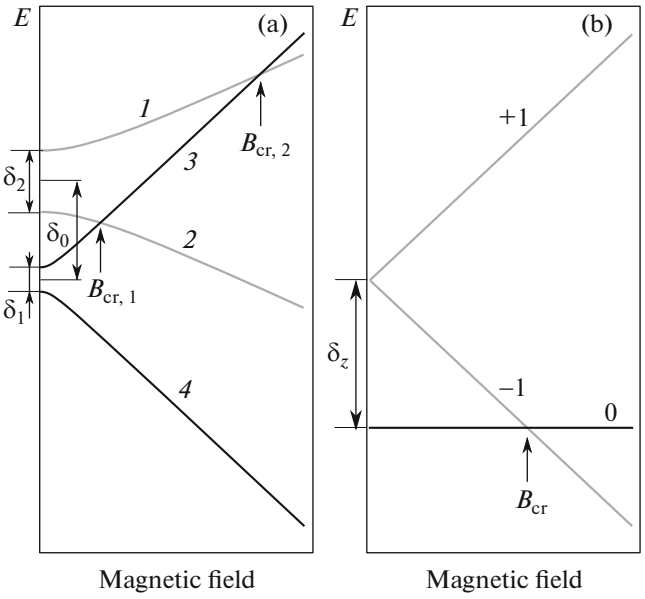

Fig. 1. Dependences of the sublevels energies of (a) a heavy-hole X_{e-hh} exciton and (b) a triplet X_{trip} exciton on the longitudinal magnetic field. Vertical arrows mark critical magnetic fields B_{cr}, at which spin sublevel anticrossing occurs.

B. Triplet exciton. This model is applicable to exciton quartets in which the singlet-triplet splitting $\Delta_{\text{S-T}}$ plays the main role in the exchange interaction. This splitting is large compared to the anisotropic splitting of triplet states with the total spin projections of the electron–hole pair $S = \pm 1$ and $S = 0$. Therefore, singlet and triplet excitons may be considered individu-

ally. In the longitudinal magnetic field, the spin Hamiltonian of the triplet exciton X_{trip} looks like

$$\mathcal{H}_{\text{exc}} = E_0 + \delta_z\left(S_z^2 - \frac{2}{3}\right) + \delta_{xy}(S_x^2 - S_y^2) + g_{\text{tr}}\mu_B B_z S_z, \quad (4)$$

where S_α are 3×3 matrices of the angular momentum $S = 1$; δ_z and δ_{xy} are exchange constants; g_{tr} is the g factor of the triplet exciton. If the localization symmetry center has an axial symmetry, then the constant δ_{xy} is zero and three sublevels of the triplet have the following energies (Fig. 1b):

$$E_{\pm 1} = E_0 + \frac{\delta_z}{3} \pm g_{\text{tr}}\mu_B B_z, \quad E_0 = E_T - \frac{2\delta_z}{3}. \quad (5)$$

2.2. MCPL in Bulk Solid Solutions and Nanostructures

Before we begin to discuss the results of experimental and theoretical investigation of the MCPL in solids, formulas will be given for the intensity and circular polarization of photoluminescence of excitons in the simplest case: (a) exchange level splitting of the exciton quartet X_{e-hh} and exciton triplet X_{trip} is neglected and (b) the spin relaxation time between the sublevels is much shorter than the exciton lifetime, so that the populations of the Zeeman sublevels are quasi-equilibrium, and the relative probability of finding the exciton in the state $|m\rangle$ is

$$f_m = \frac{\exp\left(-\frac{E_m}{k_B T}\right)}{\sum_{m'} \exp\left(-\frac{E_{m'}}{k_B T}\right)},$$

where T is the sample temperature; k_B is the Boltzmann constant; m and $m' = \pm 1, \pm 2$ for X_{e-hh} and $m = \pm 1, 0$ for the X_{trip} exciton. In this case, the intensity I and the circular polarization degree P_c of the radiation are defined as

$$I = C_I \frac{F(B_z)}{2\tau_r/\tau_{nr} + F(B_z)} G, \quad P_c = \tanh\left[\frac{(g_e - g_{hh})\mu_B B_z}{2k_B T}\right] \quad (6)$$

for the heavy-hole exciton and

$$I = C_I' \frac{F'(B_z)}{(3\tau_r/2\tau_{nr}) + F'(B_z)} G, \quad P_c = -\tanh\left(\frac{g_{\text{tr}}\mu_B B_z}{k_B T}\right) \quad (7)$$

for the triplet exciton. Here, C_I and C_I' are coefficients independent of the magnetic field, G is the exciton generation rate,

$$F(B_z) = 1 - \tanh\left(\frac{g_e\mu_B B_z}{2k_B T}\right)\tanh\left(\frac{g_{hh}\mu_B B_z}{2k_B T}\right), \quad F'(B_z) = \frac{3\cosh\left(\frac{g_{\text{tr}}\mu_B B_z}{k_B T}\right)}{1 + 2\cosh\left(\frac{g_{\text{tr}}\mu_B B_z}{k_B T}\right)}, \quad (8)$$

and the radiative and nonradiative exciton lifetimes τ_r and τ_{nr} are introduced. The time τ_{nr} is assumed to be independent of the exciton state m; the state $|0\rangle$ is regarded optically inactive in the case of the triplet exciton. As the magnetic field increases, the polarization tends to 100%; its sign is defined by the sign of the product $(g_e - g_{hh})B_z$ or $g_{\text{tr}}B_z$.

The limit value of 100% is achieved if there is no anisotropy in the plane perpendicular to the magnetic field. The cases of violated axial symmetry require special analysis. One of such cases is met in ZnSe/BeTe systems without common cation and anion, in which the heterojunction (001) belongs to the type II, and an indirect exciton formed by an electron and a hole subjected to size quantum effects in the neighbor ZnSe and BeTe layers makes a contribution into the PL. Due to anisotropy of chemical bonds at the (001) interfaces, the matrix elements of optical band-to-band transitions with polarizations [1 $\bar{1}$0] and [110] are different, and the exciton radiation in the [001] direction is linearly polarized to a degree of $P_l \sim 0.6$ [27]. In the longitudinal magnetic field, the circular polarization P_c is added to the linear polarization of the PL. Since the net polarization degree $P = \sqrt{P_l^2 + P_c^2}$ does not exceed 1, the maximal value of the circular polarization in a strong magnetic field cannot be larger than $\sqrt{1 - P_l^2} = 0.8$, which is in accordance with the experiment; for direct optical transitions the limit value of P_c was near to 100% [27].

A. Anticrossing of exciton levels in the magnetic field. In the simplest case of quasi-equilibrium distribution among the sublevels and neglecting the exchange interaction, the intensity I and polarization P_c are monotonous functions of the magnetic field. The behavior of functions $I(B_z)$, $P_c(B_z)$ allowing for the exchange interaction is quite different. The fact is that energies of some level pairs become equal in certain magnetic fields if $\delta_n \neq 0$ ($\delta_z \neq 0$). For example, level crossing for a X_{e-hh} exciton with $\delta_0 > 0$ and $\delta_1 = \delta_2 = 0$ takes place in the following magnetic fields $B \equiv |B_z|$:

$$B_{\text{cr}} = \frac{\delta_0}{2\mu_B}\begin{cases} g_e^{-1}, g_{hh}^{-1}, & \text{if} \quad g_e + g_{hh} > 0, \\ -g_e^{-1}, -g_{hh}^{-1}, & \text{if} \quad g_e + g_{hh} < 0, \end{cases}$$

where only positive values $B_{cr,1}$ and $B_{cr,2}$ should be left in the right-hand side. Therefore, if g_e and g_{hh} are equal, one of the lower ± 2 sublevels crosses one by one two upper sublevels, and if signs of g_e and g_{hh} are opposite, one of the upper sublevels crosses the lower sublevels. Expressions for the critical values $B_{cr,1}$, $B_{cr,2}$ at $\delta_1, \delta_2 \neq 0$ are given in [26]. Curves in Fig. 1a are plotted for g_e and g_{hh} of the same sign. In the triplet exciton X_{trip}, crossing of one of the $|\pm 1\rangle$ sublevels with the $|0\rangle$ sublevel occurs at the only magnetic field value (Fig. 1b):

$$B_{cr} = |\delta_z / g_{tr}\mu_B|. \quad (9)$$

Even a small perturbation lowering the symmetry of the system leads to a strong resonance mixing of close levels (i.e., anticrossing) and significantly influences the intensity and polarization of the luminescence. This is most prominent when the spin relaxation of the exciton is slowed down, and hence the population of the spin sublevels is far from equilibrium and the number of nonradiative excitons becomes bigger than of radiative ones. When anticrossing of an optically active level with an inactive level occurs, mixed states arise which have the conserved total oscillator strength but a longer lifetime. As a result, the total intensity I increases, and the degree of circular polarization undergoes a resonance change, the sign of which is defined by the sign of the optically active exciton participating in the hybridization. This behavior was distinctly observed in experiments on the low-temperature PL in structures with $GaAs/Al_xGa_{1-x}As$ quantum wells [28] and type II GaAs/AlAs superlattices [29–32].

The theory of optically detected anticrossing of exciton levels in semiconductors in the magnetic field is developed in [26]. Calculation results for the intensity and circular polarization of radiation of X_{e-hh} excitons in the type II GaAs/AlAs superlattice are shown in Fig. 2. Level anticrossing is described by introducing a low-symmetry perturbation $\hat{V}$, which mixes the radiative states with nonradiative ones. The operator $\hat{V}$ is assumed to act on the electron and hole spins independently, so that $\hat{V} = \hat{V}^e + \hat{V}^h$, $\hat{V}^e = \sigma_+ V_e + \sigma_- V_e^*$, and $\hat{V}^h = \sigma_+^h V_h + \sigma_-^h V_h^*$, where $\sigma_\pm = (\sigma_x \pm i\sigma_y)/2$, σ_α are the Pauli spin matrices; $\sigma_\pm^h = (\sigma_x^h + i\sigma_y^h)/2$, σ_α^h are the Pauli pseudo-spin matrices in the basis of the states of heavy $\pm 3/2$ holes. To allow for the quasi-resonance exciton excitation, two generation rates are introduced: G_0 for the dark states with $m = \pm 2$ and $G_0 + G_r$ for the light states with $m = \pm 1$. Experimentally found exchange constants and g factors were used in the calculation, and the ratios G_r/G_0 and τ_{nr}/τ_r were chosen to fit the best to dependence $P_c(B_z)$ measured in the GaAs/AlAs 17.4/26 Å superlattice [31]. Analysis shows that there are two different reasons for appearing of the circular polarization of the PL: (1) the difference in the generation rates of radiative and nonradiative states, and (2) difference in the lifetimes $\tau_r\tau_{nr}/(\tau_r + \tau_{nr})$ and τ_{nr} of the excitons in these states. If the first reason prevails, so that $G_0\tau_{nr} < G_r\tau_r$, then the anticrossing is accompanied by a decrease in the intensity and the absolute value of the circular polarization degree. If the difference in the lifetimes is the main factor, and $G_0\tau_{nr} > G_r\tau_r$, then the anticrossing leads to pumping of the excitation from a more populated nonradiative state 3 to a less populated state $j = 1$ or 2 (Fig. 1a), and as a result, the total intensity I and magnitude of P_c increase. With the chosen parameters, the inequality $G_0\tau_{nr} > G_r\tau_r$ is true, and hence the second scenario takes place (see Figs. 2a and 2b) in accordance with the experiment on the analysis of the circular polarization in the longitudinal magnetic field [30–32].

Copper-doped GaP crystals. In these materials the triplet exciton X_{trip} is bound on a deep impurity center and emits a photon with the energy of 1.911 eV, which differs noticeably from the low-temperature width of the indirect energy gap—2.32 eV. For one of the samples, the exciton parameters met in Eq. (4) and determined from comparison with the experimental data were $g_{tr} = 2.05$, $\delta_z = +0.013$ meV, $\delta_{xy} = 0.0025$ meV [12]. According to Eq. (9), level anticrossing should happen at $B \sim 0.1$ T. In the experiment carried out in [12], the PL intensity increases as the field increases, attains the maximum near 0.1 T, and then decreases. Apparently, it was the first observation of exciton level anticrossing in semiconductors.

$CdS_{1-x}Se_x$ solid solutions. In low-temperature spectra of photoluminescence of solid solutions with substitutions in the anion sublattice, a wide band of radiative recombination of excitons localized on composition fluctuations, and its LO replica are observed. In semiconductors having the wurtzite structure (CdS, CdSe) the ground exciton state consists of a heavy hole, and the localized exciton belongs to the class X_{e-hh}. Data on the PL polarization at resonance excitation of the excitons by linearly and circularly polarized light show that a hidden anisotropy is present in the system of fluctuation excitons: there is not only a splitting between the ± 1 and ± 2 doublets ($\delta_0 \neq 0$), but also between the sublevels of the light exciton ($\delta_2 \neq 0$) [13, 33]. Oscillating dipolar moments of excitons at these sublevels, the sublevels 1 and 2 in Fig. 1a, are oriented along the axes η and ξ, which are distributed randomly in the plane perpendicular to the principal axis $z \parallel C_6$. The spin Hamiltonian parameters were determined from the nonmonotonous behavior of the polarization degree $P_c(B)$, caused by the exciton level anticrossing [34]: $\delta_0 = 0.62$ meV, $\delta_2 = 0.25$ meV, $g_e = 1.8$, and $g_{hh} = 5.7$.

GaSe crystals and $GaSe_{1-x}Te_x$ solid solutions. Localized excitons in these materials have the fine

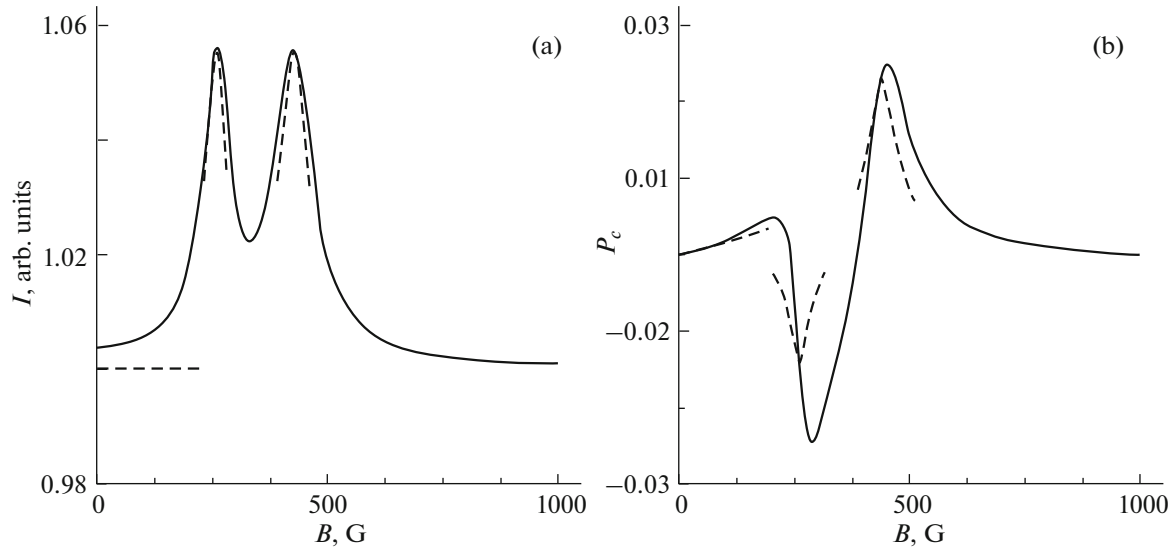

Fig. 2. Dependences of the (a) total intensity and (b) circular polarization degree of exciton luminescence in the type II GaAs/AlAs superlattice on the longitudinal magnetic field B_z. Solid curve represents an exact calculation; dashed lines, calculation in the approximation of an isolated level pair or in the weak fields. The following parameters were used: $\delta_0 = 4.5$ μeV, $\delta_1 = 0$, $\delta_2 = 2$ μeV, $|V_e| = 0.3$ μeV, $V_h = 0$, $g_e = 2.08$, $g_{hh} = 0.83$, $G_r/G_0 = 2$, $\tau_{nr}/\tau_r = 4$, spin relaxation was neglected (see [26]).

structure of triplet excitons X_{trip}. Time-resolved spectroscopy was used in [35, 36] to study the time dependence of the signal of Zeeman sublevels anticrossing in the radiation from localized triplet excitons in a GaSe crystal and $GaSe_{1-x}Te_x$ solid solution in the longitudinal magnetic field with nonpolarized pumping.

At a stationary optical excitation, the dependence of the photoluminescence intensity I on the magnetic field B at a fixed radiation wavelength has a maximum that is the signal of the level anticrossing. When excited by a short pulse, the shape of this signal changes remarkably during the time t counted from the moment of the excitation. At $t = 0$ the anticrossing signal is very weak; as t increases, a maximum appears in the field dependence of the exciton radiation intensity (at this stage, the shape of the anticrossing signal is analogous to the shape observed under stationary excitation). At further increase of t the dependence $I(B)$ turns to a double-maximum curve. A local perturbation V was introduced in the theoretical description of the intensity time evolution $I(t)$ in [35, 36]; it was determined by the matrix elements $\langle m'|V|m\rangle$ ($m' \neq m$) and mixed the states $|1\rangle$, $|0\rangle$, and $|-1\rangle$. The best agreement with the experiment was obtained with the following parameter sets: $\delta_z = 0.0357$ meV, $g_{\text{tr}} = 1.7$, $\tau_r = 0.125$ μs, $\tau_{nr} = 7$ μs, $2|\langle 0|V|\pm 1\rangle| = 0.0045$ meV for GaSe and $\delta_z = 0.05$ meV, $g_{\text{tr}} = 1.85$, $\tau_r = 0.16$ μs, $\tau_{nr} = 10$ μs, and $2|\langle 0|V|\pm 1\rangle| = 0.008$ meV for $GaSe_{0.87}Te_{0.13}$.

Structures with quantum dots and nanocrystals. As the dimensionality lowers, overlap of the electron-hole envelopes grows, and hence the exchange interaction increases. That is why the exchange constant δ_0 for excitons X_{e-hh} in quantum dots varies in a wide range and can achieve several millielectronvolts [19, 37].

As an initial model for the preliminary analysis of experimental data we can use the model from Section 2.A, in which the relaxation from upper (light) sublevels 1, 2 to lower (dark) sublevels is regarded, and the inverse processes are neglected. In this case for the MCPL degree of the light excitons we have

$$P_c = \frac{(g_e - g_{hh})\mu_B B_z}{\varepsilon} \frac{\tau}{\tau + \tilde{\tau}_s} \tanh\left(\frac{\varepsilon}{2k_B T}\right). \qquad (10)$$

Here $\varepsilon = \sqrt{[(g_e - g_{hh})\mu_B B_z]^2 + \delta_2^2}$, $\tilde{\tau}_s = 2\tau_s[1 + \exp(-\varepsilon/k_B T)]^{-1}$; τ is the lifetime of the exciton states 1, 2; τ_s is the spin relaxation time between them defined so that the $1 \to 2$ transition rate from the upper to the lower sublevel is $f_1/2\tau_s$, and the rate of transitions $2 \to 1$ is $f_2\exp(-\varepsilon/k_B T)/2\tau_s$ (where f_1 and f_2 are the populations). This model is applicable for many structures with quantum wells (see [38–41]). In some cases, however, more complicated models should be used. For example, the MCPL of excitons may be influenced by the shape of a colloid CdTe nanocrystal—either elongated or oblate spheroid [42].

It is possible to observe exciton sublevel anticrossing in quantum dots with small values of δ_0; an example is the structure with self-organized InP quantum dots with $\delta_0 = 0.14$ meV [43]. On the other hand, in spherical nanocrystals and in the "dot-in-a-rod" CdS/CdSe nanoobjects the exchange constant δ_0 is 2–5 meV, and anticrossing is possible only in very strong

fields; moreover, X_{e-hh} excitons at a low temperature gather only on the lower, dark sublevels 3, 4 and produce luminescence only due to violations of standard selection rules [19].

2.3. Dynamics and Kinetics of Light and Dark Excitons in an Ultrathin GaAs/AlAs Quantum Well

The MCPL of excitons and many-exciton complexes in bulk semiconductors with an indirect band gap Ge and Si were investigated in detail in the 1970s. Results of these studies were presented in the review chapter 6 of a multiauthor monograph [44]. We will consider this phenomenon and also the dependence of the PL intensity on the magnetic field in a structure with one monomolecular layer of GaAs placed between 50-nm AlAs layers [20, 21] (see also the paper by Shamirzaev in this issue [22]). This structure is two times indirect: both in the real space and in the **k**-space; a X_{e-hh} exciton localized there consists of a Γ-hole in the GaAs layer and an electron from the X_x, X_y valleys in the AlAs layers, bound to the hole by Coulomb interaction. Since the g factors of the electron and holes are of the same sign ($g_e, g_{hh} > 0$), the excitons are accumulated on the optically inactive sublevel +2 or −2 at a low temperature in a strong longitudinal magnetic field. Therefore, they experience mostly nonradiative recombination, and the PL is weakened; since the times of the radiative and nonradiative exciton recombination differ significantly ($\tau_{nr} \gg \tau_r$), the decay kinetics of the low-temperature PL is slow. Figure 3a shows that the PL intensity decreases monotonously without the field. In the magnetic field of 9 T the dependence $I(T)$ is quite different (Fig. 3b): as the temperature rises, the relative population of the light sublevels increases, and thus the PL intensity grows and its kinetics become faster. For instance, the intensity grows several times as the temperature changes from 2 to 7 K. At even higher temperatures, the role of nonradiative recombination becomes more important, and the intensity I begins to decrease. Remember that this behavior of the PL is typical of the excitons with g_e and g_{hh} having the same sign. If the signs of the g factors are opposite (like in the structure with a CdTe/CdMgTe quantum well), then the PL intensity remains high in magnetic fields up to $B = 45$ T [45].

To describe the dependences $I(B, T)$ and $P_c(B, T)$, a theory of stationary and time-resolved PL of localized excitons was developed in [20, 21]. Since in the studied type II nanostructures the exchange interaction is weak and the measurements were carried out in relatively low magnetic fields, the exchange splitting was neglected, and only the Zeeman contribution (2) into the exciton spin Hamiltonian was considered. Curved arrows in Fig. 3c show the relaxation processes between exciton sublevels; transitions with spin changes of only one particle are taken into account: $|s, j\rangle \to |-s, j\rangle$ or $|s, j\rangle \to |s, -j\rangle$. The influence of the magnetic field on the probabilities of transitions from the upper to the lower levels ($W_{-1/2,\,1/2}$ and $W_{-3/2,\,3/2}$ in Fig. 3c) was neglected, and Boltzmann factors were used for the low-to-up transitions:

$$\begin{aligned} W_{1/2,-1/2} &= \alpha W_{-1/2,1/2}, \quad \alpha = \exp\left(-\frac{g_e \mu_B B}{k_B T}\right), \\ W_{3/2,-3/2} &= \beta W_{-3/2,3/2}, \quad \beta = \exp\left(-\frac{g_{hh} \mu_B B_z}{k_B T}\right). \end{aligned} \tag{11}$$

Here the general case of a slanted magnetic field **B** making the angle of θ with the axis z is considered. Expressions for α and β, respectively, include the total magnetic field B and its projection on the axis z (assumed to be positive), since the electron g factor is almost isotropic, and the effect of the lateral field projection on the heavy hole spin is neglected. That is why the symbol s in the considered case stands for the spin projection on the field direction, and j designates the projection of the hole spin on the field direction. Instead of the symbol f_{sj} for the population of the exciton sublevel, we use f_{kl}, where $k = \mathrm{sgn}(s)$ and $l = \mathrm{sgn}(j)$. The system of kinetic equations for f_{kl} may be presented as follows:

$$\begin{aligned} &\frac{df_{--}}{dt} + (D^2 w + w')f_{--} + w_e(\alpha f_{--} - f_{+-}) \\ &\qquad + w_h(\beta f_{--} - f_{-+}) = G_{--}, \\ &\frac{df_{++}}{dt} + (D^2 w + w')f_{++} + w_e(f_{++} - \alpha f_{-+}) \\ &\qquad + w_h(f_{++} - \beta f_{+-}) = G_{++}, \\ &\frac{df_{+-}}{dt} + (C^2 w + w')f_{+-} + w_e(f_{+-} - \alpha f_{--}) \\ &\qquad + w_h(\beta f_{+-} - f_{++}) = G_{+-}, \\ &\frac{df_{-+}}{dt} + (C^2 w + w')f_{-+} + w_e(\alpha f_{-+} - f_{++}) \\ &\qquad + w_h(f_{-+} - \beta f_{--}) = G_{-+}. \end{aligned} \tag{12}$$

Here $w = 1/\tau_r$ and $w' = 1/\tau_{nr}$, $w_e = W^{-1}_{-1/2,1/2}$ and $w_h = W^{-1}_{-3/2,3/2}$; $C = \cos(\theta/2)$ and $D = \sin(\theta/2)$; G_{kl} is the exciton generation rate on the k, l sublevel. At the nonresonance excitation this rate can be assumed the same for all sublevels: $G_{kl} \equiv G$. The PL intensities with the right- and left-hand polarization are related to the populations f_{kl} as

$$I_{+/-} \propto \frac{C^2}{\tau_r} f_{-+/+-} + \frac{D^2}{\tau_r} f_{++/--}, \tag{13}$$

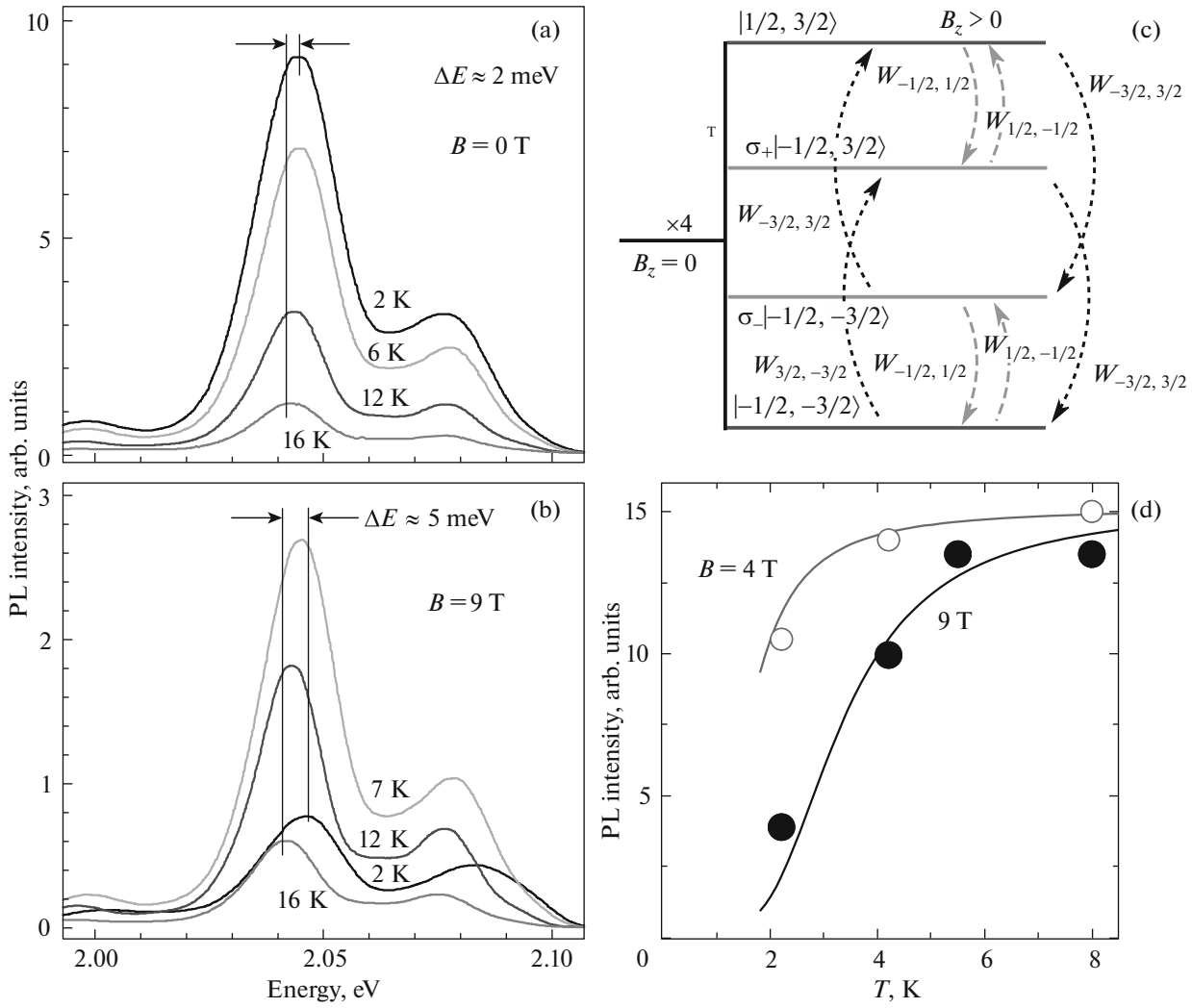

Fig. 3. PL spectra of an ultrathin quantum well GaAs/AlAs QW measured in the Faraday geometry at four temperatures: (a) $B = 0$ and (b) 9 T. (c) Schematic diagram of the considered transitions (with emission or absorption of phonons) between the exciton sublevels split in the magnetic field. (d) Temperature dependence of the PL intensity at $B = 4$ and 9 T (circles). Solid lines were obtained in the slope of the kinetic theory [20] with the following parameters: $\tau_r = 0.34$ ms, $\tau_{nr} = 8.5$ ms, $g_e = 2$, $g_{hh} = 3.5$, $w_e = w_h = 1.25 \times 10^5$ s^{-1} [20].

and hence the expression for the polarization degree can be derived:

$$P_c = \frac{C^2(f_{-+} - f_{+-}) + D^2(f_{++} - f_{--})}{C^2(f_{-+} + f_{+-}) + D^2(f_{++} + f_{--})}. \qquad (14)$$

In a detailed comparison with the experimental data in [21], a small violation of the selection rules was allowed for, and Eq. (14) was slightly modified.

In Fig. 3d the calculation results are compared with the experiment on thermal activation of the exciton PL. Figure 4 demonstrates the recombination dynamics of formation of the MCPL in the longitudinal and slanted magnetic fields. Analysis shows that the buildup time of the absolute value $|P_c|$ is defined solely by the smallest of the spin relaxation times $(2w_e)^{-1}$ and $(2w_h)^{-1}$, and the sign of P_c is defined by the ratio w_h/w_e, which was much bigger than unity in the studied samples. At the low temperature, the MCPL shows an unusual nonmonotonous angular dependence $P_c(\theta)$ (Fig. 5).

2.4. MCPL of Excitons and Trions in Two-Dimensional Systems

Interaction of excitons with charge carriers, electrons or holes, in two-dimensional semiconductor systems leads to formation of three-particle charged complexes, a trion X^- [46] (an analogue of the negatively charged hydrogen ion H^- [7]) consisting of two electrons and one hole or a trion X^+ made of two holes and one electron. In low-temperature PL spectra of

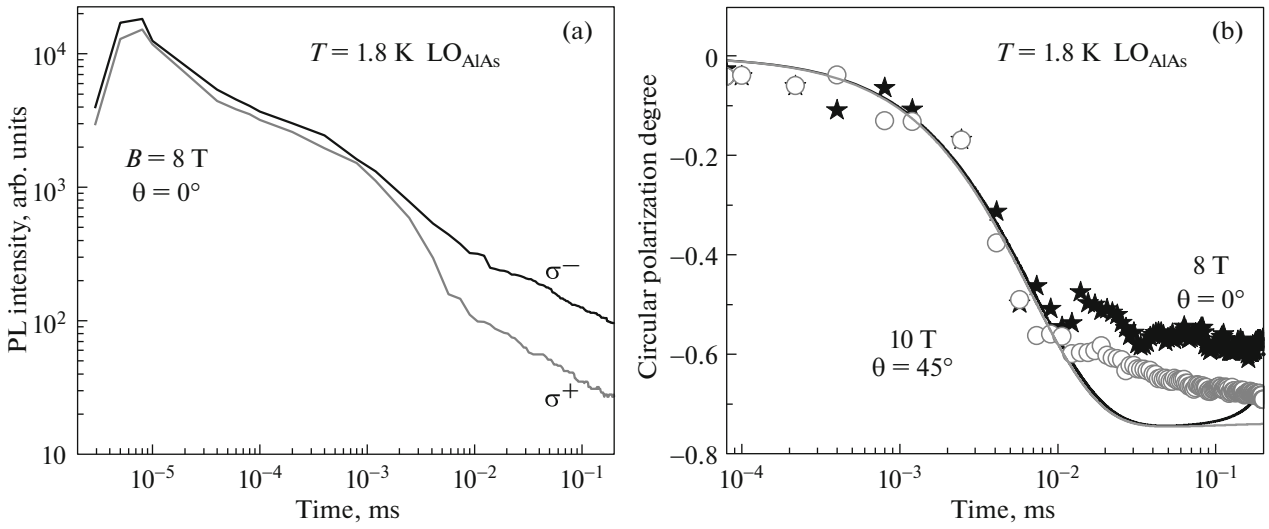

Fig. 4. (a) Time course of decays of the σ_+ and σ_- components of the LO_{AlAs} phonon replica of the PL at pulsed optical pumping in the Faraday geometry at $B = 8$ T and the temperature of 1.8 K. (b) Appearing of the circular polarization in the LO_{AlAs} radiation line in time. Stars and circles show the experiment at $B = 8$ T in the Faraday geometry and at $B = 10$ T in the slanted field (angle $\theta = 45°$), respectively [21].

alloyed 2D structures (and in some cases also of structures which were not alloyed intentionally) two lines are observed, one from excitons and one from trions (see [47–51]).

A. Coexisting of excitons and trions in quantum wells. Without magnetic field or in a relatively weak field the spins of two identical particles are antiparallel, and the exchange interaction between them and the spin of the unpaired particle is absent. The MCPL of trions is defined by the selective population of the spin sublevels of the unpaired particle, and for heavy-hole trions it is described by the formulas

$$P_c(X_{hh}^-) = -\frac{\tau}{\tau + \tilde{\tau}_{s,hh}} \tanh\left(\frac{\varepsilon_{hh}}{2k_B T}\right),$$
$$P_c(X_{hh}^+) = \frac{\tau}{\tau + \tilde{\tau}_{s,e}} \tanh\left(\frac{\varepsilon_e}{2k_B T}\right). \quad (15)$$

Here $\varepsilon_{hh} = g_{hh}\mu_B B_z$, $\varepsilon_e = g_e \mu_B B_z$, and at ε_e, $\varepsilon_{hh} > 0$ we have

$$\tilde{\tau}_{s,hh} = 2\tau_{s,hh}[1 + \exp(-\varepsilon_{hh}/k_B T)]^{-1},$$
$$\tilde{\tau}_{s,e} = 2\tau_{s,e}[1 + \exp(-\varepsilon_e/k_B T)]^{-1},$$

where $\tau_{s,e}$ and $\tau_{s,hh}$ are the spin relaxation times of the electron and the heavy hole. In deriving Eq. (15) the trion generation rate was assumed independent of the spin state of the trion. In this case, the circular polarization signs of the PL of the exciton, trion X^- and trion X^+ are defined by the signs of $g_e - g_{hh}$, $-g_{hh}$, and g_e, respectively. In particular, this means that if the signs of $g_e - g_{hh}$ and $-g_{hh}$ are opposite, the polarization degrees of the exciton and the X^- trion are also opposite, as it was observed in PL spectra of the $CdTe/Cd_{0.7}Mg_{0.3}Te$ quantum well [48]. As the magnetic field grows, the g factor of the heavy hole in this structure changes its sign at $B = 12$ T, and the polarization orientation $P_c(X_{hh}^-)$ changes consequently.

Longitudinal magnetic field influences drastically the distribution of PL intensity of excitons and trions.

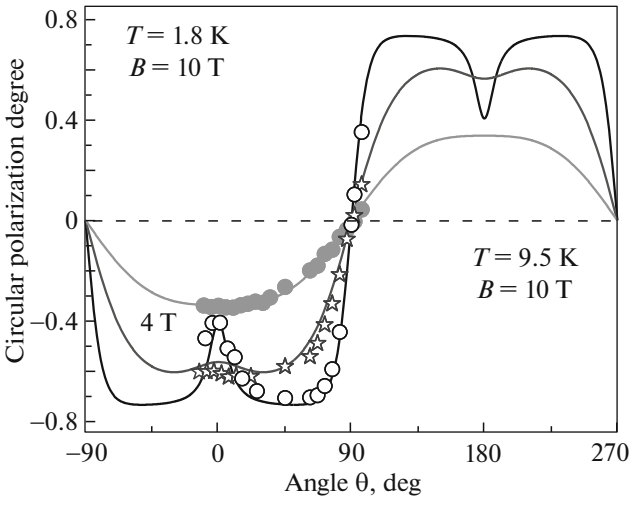

Fig. 5. Angular dependence of the MCPL $P_c(\theta)$ measured at $T = 1.8$ K for $B = 4$ T (stars) and 10 T (empty circles), and also for $T = 9.5$ K and $B = 10$ T (filled circles). The curves were calculated using the model (12) with $\tau_r = 0.34$ ms, $\tau_{nr} = 8.5$ ms, $\tau_{se} = (2w_e)^{-1} = 33$ μs, $\tau_{sh} = (2w_h)^{-1} = 3$ μs [21].

First, it is caused by the fact that a singlet trion can appear only if the spin of the resident electron and the electron in the exciton have opposite spins. Second, spin sublevels of the exciton have selective populations in the magnetic field, and temperature alters these populations. For example, in the $CdTe/Cd_{0.7}Mg_{0.3}Te$ quantum well in the zero field at $T = 1.6$ K the exciton PL line is weaker than the trion line, but at $B = 5$ T the exciton and trion contributions into the σ_- component of the PL become comparable [45]. As the temperature rises from 1.6 to 16 K, the population redistribution of the exciton sublevels makes the trion line dominant again [50]. In very intense fields, a triplet trion with the total spin of paired electrons $S = 1$ becomes visible in the PL spectra [45, 52].

Note the similarity of the MCPL phenomenon in excitons bound on neutral donors in bulk semiconductors and in trions in structures with quantum wells, grown on the basis of these semiconductors [11, 53].

B. MCPL in two-dimensional transition metals dichalcogenides. In recent years two-dimensional semiconductor compounds of a new class have been actively studied: transition metals dichalcogenides with the chemical formula MX_2, where M is molybdenum or tungsten, and X is sulfur or selenium. They possess a direct energy gap in the visible optical band. The bottom of the conduction band and the top of the valence band are in the K_+ and K_- vertices of the hexagonal Brillouin zone; exciton lines are observed in the PL spectrum even at the room temperature. In addition to the exciton line, the trion luminescence is also observed.

Monomolecular MX_2 layers are characterized by the point symmetry D_{3h}, and the point symmetry of the wave vector group K_+ or K_- is C_{3h}. In the C_{3h} symmetry the spin-orbital interaction removes totally the spin degeneracy in the extremum points; according to the time inversion symmetry, the spin splitting in the K_+ and K_- valleys has opposite signs. In all four materials MoS_2, WS_2, $MoSe_2$, and WSe_2 the spin splitting Δ_v of the valence band is larger than 100 meV, and the splitting Δ_c is on the order of several meV or several dozen millielectronvolts [54, 55]. In molybdates the signs of Δ_c and Δ_v are opposite, and in tungstates they are the same. Band-to-band optical transitions conserve the spin for light having the circular polarization σ_+ in one valley and σ_- in the other valley. In what follows, we consider the exciton transitions involving a hole in the ground spin state (A-excitons). These transitions are optically active for an electron also in the ground state, if Δ_c and Δ_v have different signs. If the signs of the spin splittings coincide, then the exciton state with the electron on the upper spin sublevel is the light one. In both cases, however, measurement of the circularly polarized PL component allows determining the contribution of a certain valley into the secondary radiation.

In the longitudinal magnetic field, the Zeeman energy $(g_e s_z^e + g_h s_z^h)\mu_B B_z$ is added to the exciton energy, the peak of the $\sigma_\pm$ exciton luminescence band shifts by $\pm\delta_Z/2$, so that the relative shift of these bands is δ_Z, and $\delta_Z = |(g_e - g_h)\mu_B B_z|$. A comparative study of the magnetooptical properties of 2D molybdenum and tungsten diselenides was performed in [56]. Obtained polarized PL spectra are shown in Fig. 6. In the $MoSe_2$ single layer the magnetic circular polarization is observed in both exciton and trion bands (Fig. 6a), while in WSe_2 the integral intensity of the trion band in the magnetic field remains unpolarized (Fig. 6d). The difference in the behavior of excitons in these materials is explained by different signs of Δ_c in them. In the $MoSe_2$ single layer the exciton ground state is the light one, and part of the excitons go from the valley with the positive Zeeman energy $\delta_Z/2$ to the valley with the energy $-\delta_Z/2$ during their lifetime. In the WSe_2 a light exciton (which is the excited state) goes to the optically inactive ground state before the transition to the other valley can happen.

In the experiment described in [57] it was possible to alter the alloying level of the WSe_2 single layer and go from a *p*-type sample to an *n*-type sample through the case of a sample with zero concentration of charge carriers. The binding energy of the X^+ trion was found to be 21 meV, and the X^- trion appeared as two spectral peaks with the binding energies of 29 and 35 meV. Analysis shows that the X^+ trion, which makes its contribution into the PL, consists of two holes in the singlet state and placed one in the K_+ valley and other in the K_- valley, and an unpaired electron in the upper spin state [57]. The luminescence peaks of the X^- trion were found to be due to the following three-particle states: (1) two electrons with opposite spins and an unpaired hole in the same valley, and (2) electrons with parallel spins but in different valleys (i.e., one electron in the ground spin state and the other in the excited state) and an unpaired hole in the valley where the electron in the upper spin state resides.

2.5. Additional MCPL Mechanisms Related to Excitons

In this section we will consider briefly special mechanisms of the circular polarization appearing in the exciton luminescence.

A. Exciton magnetic polarons. In semimagnetic semiconductors the exchange interaction of localized charge carriers with magnetic ions leads to formation of an exciton magnetic polaron. In a bulk sample polaron of this kind may appear only if the initial nonmagnetic localization is strong enough, whereas just a small initial localization of an exciton is sufficient for formation of a magnetic polaron in a two-dimensional structure [58].

Investigation of the MCPL allows obtaining an independent estimate of the sizes of a magnetic

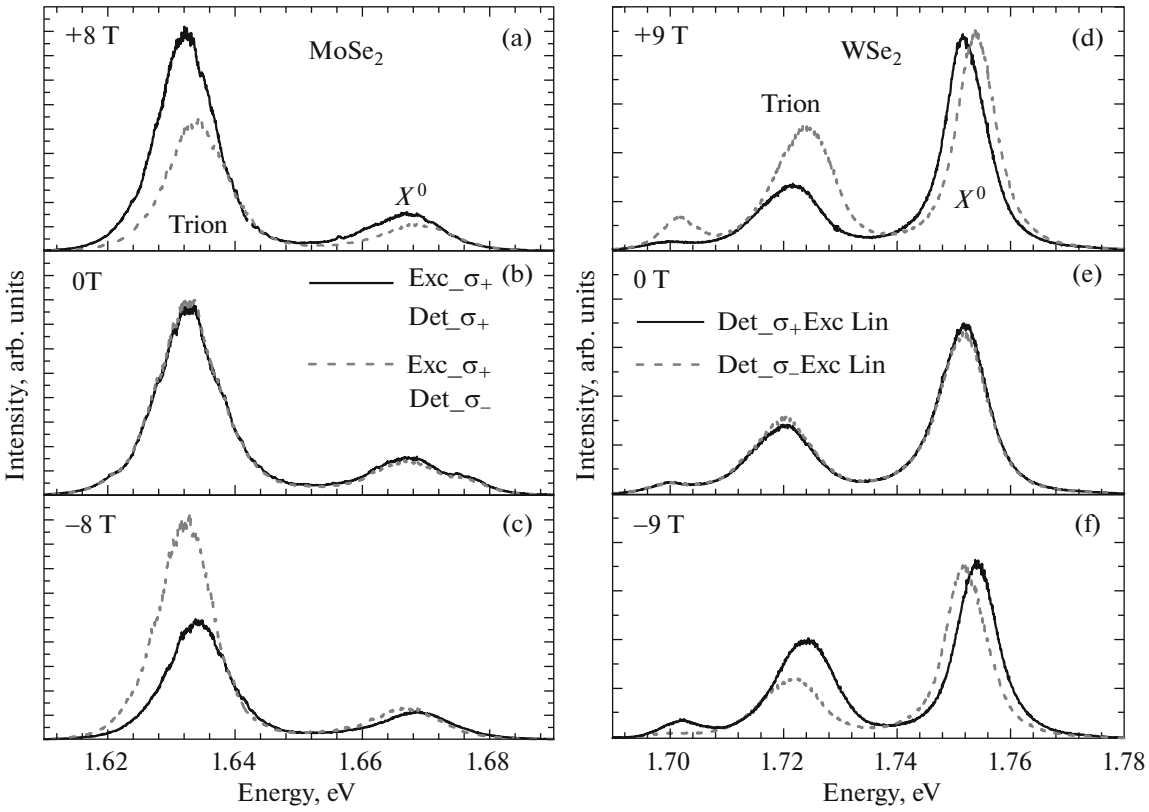

Fig. 6. PL spectra measured at the σ_+ (solid curves) and σ_- (dotted curves) polarizations in a $MoSe_2$ single layer with circularly polarized excitation (left panel) and in a WSe_2 single layer with linearly polarized excitation (right panel). Panels (b, e) present the experiment performed without the magnetic field; (a, c), at $B_z = 8$ and -8 T; (d) and (f), at $B_z = 9$ and -9 T [56].

polaron. Three methods of obtaining the polaron radius r_0 in epitaxial layers of $Cd_{1-x}Mn_xTe$ were used in [59]. The polarization method relied on the fact that the polaron volume $V = (4\pi/3)r_0^3$ is related to the derivative $\theta = (dP_c/dB_z)_{B_z=0}$ of the PL circular polarization with respect to the magnetic field according to the Eq. (7) in [59]:

$$V = \frac{\pi k_B T \theta^2}{2\chi}, \qquad (16)$$

where χ is the contribution of magnetic ions to the spin susceptibility in the absence of the magnetic field. In samples with the composition $x = 0.07$–0.39 the derivative θ decreased from 4.44 to 1.05. Obtained dependence of r_0 on x was in a good agreement with the definition of r_0 from estimates of the magnetic polaron by Eq. (4) in [59]. Measuring the value of $\theta = 9.2$ T^{-1} in the $Cd_{0.935}Mn_{0.065}Te/Cd_{0.83}Mg_{0.17}Te$ quantum wells allowed determining the energy of the magnetic polaron to be $E_{MP} = 13 \pm 3$ meV, which agrees with $E_{MP} = 12 \pm 1$ meV found from measurement of the difference between the photon energy and the spectral peak of the secondary radiation in the resonance optical excitation of localized excitons [58]. Nonmagnetic contribution into the exciton localization energy was found to be only 4 meV. Analysis of the field dependence of the MCPL allowed distinguishing two modes of the PL induced by the external magnetic field, which were called the "paramagnetic" and "spin-glass" phases in [60].

B. Exciton polaritons in the longitudinal magnetic field. Exciton polaritons in planar optical microcavities possess an important feature: the component of the polariton wave vector in the plane of the structure is conserved when the polaritons tunnel through the mirror (distributed Bragg reflector) into vacuum and are transformed into photons. That is why the distribution and dynamics of exciton polaritons can be studied experimentally using reflection, scattering, transmission, and luminescence by making spectral measurements of the light intensity emitted from the microcavity at different angles. Exciton polaritons in a microcavity, being bosons, may experience condensation similar to the Bose–Einstein condensation when their free motion is restricted in space and the critical conditions are achieved (see, for example, a review [61]).

A polariton with a X_{e-hh} exciton has the spin degree of freedom; circularly polarized states correspond to the spin projections ± 1. Due to the exchange interac-

tion between particles, the ground state of the condensed exciton phase is linearly polarized, i.e., coherent superposition of the circular components σ_+ and σ_-. MCPL studied in [62] revealed that the Zeeman splitting of spin components is suppressed until some threshold magnetic field is attained in the spinor condensate of exciton polaritons in a microcavity with GaAs quantum wells and $Al_{0.2}Ga_{0.8}As/AlAs$ Bragg mirror. The mentioned field threshold value is defined by the difference of the interaction energies between bosons with the same and opposite spin orientations. Another behavior of polariton condensate in a similar structure was observed in [63]: condensation for each of the spin components occurred at different critical powers Q_{th}, and the difference of the critical values $Q_{th}^- - Q_{th}^+$ for the σ_- and σ_+ components decreased with the magnetic field. Measurements of the dependence of the splitting of the spin-polarized polariton states on the laser pumping power density in the magnetic field showed that the changes are within the experiment accuracy level and do not exceed 15% of the splitting value [64]. The weak dependence of the Zeeman splitting on the pumping observed in [65] is explained by a slow spin relaxation between the spin sublevels and also by the fact that the system, consisting of the exciton gas in a reservoir and polariton condensate, is far from the thermodynamic equilibrium. Photoluminescence spectra of exciton polaritons in microcavities as a function of the optical excitation density and the magnetic field were investigated in [65]. It was found that at exciton concentration rising and constant magnetic field or at increasing field and fixed exciton concentration, all excitons are gathered on the bottom spin energy level, though the Zeeman splitting is only 0.15 meV and is smaller than the thermal energy $k_BT = 0.5$ meV. This is possible if the chemical potential of the system of exciton polaritons turns to zero, that is, if they are condensed.

C. PL polarization of paraexcitons in Cu_2O in the magnetic field. The ground state of an exciton $\Gamma_6^+ \times \Gamma_7^+$ is split by the exchange interaction into an ortho- and paraexciton. In the paraexciton, the spins of the electron and hole are antiparallel, and the total spin is zero. This exciton state Γ_2^+ is not degenerate, does not undergo Zeeman splitting in the magnetic field, and thus one cannot expect to obtain circular polarization of the paraexciton radiation. Nevertheless, Gastev et al. observed circular polarization induced by the magnetic field in the B_1 band of the phonon replica accompanied by emitting of a Γ_5^- phonon [17]. The transition matrix element for the Γ_2^+ exciton may be written in the following form, allowing for the terms linear with respect to the field **B**:

$$M(\Gamma_2^+) = F(\mathbf{e}^* \cdot \mathbf{u}) + iG(\mathbf{B} \cdot [\mathbf{e}^* \times \mathbf{u}]), \qquad (17)$$

where **e** is the polarization vector of emitted light; u_x, u_y, and u_z are the amplitudes of the representation phonons Γ_5^- obeying to the transformations $x(y^2 - z^2)$, $y(z^2 - x^2)$, $z(x^2 - y^2)$; F and G are real-number coefficients. The value of F is small because the matrix element (17) at $B = 0$ is nonzero only due to spin-orbital mixing of wave functions from other bands to the Γ_6^+ and Γ_7^+ states. Equation (17) predicts that the intensities of the right- and left-hand polarized PL components in the field direction are proportional to $(F \mp GB)^2$, and the circular polarization degree is

$$P_c(B_1) = -\frac{2FGB}{F^2 + G^2B^2}.$$

The reason for appearing linear with B terms in the matrix element (17) lies in the magnetic-field-induced mixing of the paraexciton state Γ_2^+ with the orthoexciton states Γ_5^+, for which transitions with emission of Γ_5^- phonons are allowed and are not infinitesimal at $B = 0$.

CONCLUSIONS

In the past four decades, magnetic circular polarization of exciton photoluminescence has grown into a separate field of the exciton physics. Basic mechanisms of the MCPL have been revealed. Certainly, it is unnecessary to use the theory of polarized photoluminescence of a large ensemble of exciton localization centers or quantum dots, if one investigates very narrow exciton lines of an individual quantum dot by means of modern optical microspectroscopy. Nevertheless, this theory is still relevant. Technology development leads to the appearance of new semiconductor systems, and modification of the well-established mechanisms, and even the creation of additional MCPL mechanisms is necessary to describe polarization of radiation of these new objects. The advantage of the MCPL method is its relative simplicity: (a) to determine the circular polarization degree one needs only to place a circular analyzer before the detector and measure the radiation intensity at two orientations of the analyzer; (b) unlike optical orientation, this approach does not require resonance excitation; (c) spectral resolution of Zeeman sublevels is not necessary, and thus the method can be applied to a wide range of objects having broad spectral PL lines or bands; (d) though simple, it can yield a lot of information on g factors, lifetimes, and relaxation times of excitons; and (e) it is convenient for identification of exciton complexes.

ACKNOWLEDGMENTS

The work is supported by the Russian Science Foundation (project no. 14-12-01067). Author is grateful to S.Yu. Verbin, M.M. Glazov, V.P. Kocheres-

hko, A.N. Reznitskii, and D.R. Yakovlev for useful discussions of the manuscript.

REFERENCES

1. Ya. I. Frenkel', Zh. Eksp. Teor. Fiz. **6**, 647 (1936); Usp. Fiz. Nauk **93**, 408 (1967).
2. A. S. Davydov, Izv. Akad. Nauk SSSR, Ser. Fiz. **12**, 608 (1948).
3. S. I. Pekar, *Selected Works* (Naukova. Dumka, Kiev, 1988) [in Russian].
4. E. F. Gross, Usp. Fiz. Nauk **63**, 576 (1957).
5. E. I. Rashba, in *Excitons*, Ed. by E. I. Rashba and M. D. Sturdge (North-Holland, Amsterdam, 1982), Chap. 13.
6. E. F. Gross, B. S. Razbirin, and M. A. Yakobson, Sov. Tech. Phys. **2**, 1043 (1957).
7. M. A. Lampert, Phys. Rev. Lett. **1**, 450 (1958).
8. J. R. Haynes, Phys. Rev. Lett. **4**, 361 (1960).
9. R. E. Dietz, D. G. Thomas, and J. J. Hopfield, Phys. Rev. Lett. **8**, 391 (1962).
10. D. G. Thomas and J. J. Hopfield, Phys. Rev. **128**, 2135 (1962).
11. A. V. Rodina, M. Strassburg, M. Dworzak, U. Haboeck, A. Hoffmann, A. Zeuner, H. R. Alves, D. M. Hofmann, and B. K. Meyer, Phys. Rev. B **69**, 125206 (2004).
12. H. P. Gislason, B. Monemar, P. J. Bean, B. C. Herbert, S. Depinna, B. C. Cavenett, and N. Killoran, Phys. Rev. B **26**, 827 (1982).
13. S. Pemogorov, A. Reznitsky, S. Verbin, and V. Lysenko, Solid State Commun. **47**, 5 (1983).
14. D. Gammon, E. S. Snow, B. V. Shanabrook, D. S. Katzer, and D. Park, Phys. Rev. Lett. **76**, 3005 (1996).
15. S. V. Gupalov, E. L. Ivchenko, and A. V. Kavokin, J. Exp. Theor. Phys. **86**, 388 (1998).
16. K. J. Moore, G. Duggan, P. Dawson, and C. T. Foxon, Phys. Rev. B **38**, 5535 (1988).
17. R. Heitz, M. Grundmann, N. N. Ledentsov, L. Eckey, M. Veit, D. Bimberg, V. M. Ustinov, A. Yu. Egorov, A. E. Zhukov, P. S. Kop'ev, and Zh. I. Alferov, Appl. Phys. Lett. **68**, 361 (1996).
18. Feng Liu, L. Biadala, A. V. Rodina, D. R. Yakovlev, D. Dunker, C. Javaux, J.-P. Hermier, A. L. Efros, B. Dubertret, and M. Bayer, Phys. Rev. B **88**, 035302 (2013).
19. B. Siebers, L. Biadala, D. R. Yakovlev, A. V. Rodina, T. Aubert, Z. Hens, and M. Bayer, Phys. Rev. B **91**, 155304 (2015).
20. T. S. Shamirzaev, J. Debus, D. R. Yakovlev, M. M. Glazov, E. L. Ivchenko, and M. Bayer, Phys. Rev. B **94**, 045411 (2016).
21. T. S. Shamirzaev, J. Rautert, D. R. Yakovlev, J. Debus, A. Yu. Gornov, M. M. Glazov, E. L. Ivchenko, and M. Bayer, Phys. Rev. B **96**, 035302 (2017).
22. T. S. Shamirzaev, Phys. Solid State **60** (2018, in press).
23. S. V. Gastev, E. L. Ivchenko, G. E. Pikus, N. S. Sokolov, and N. L. Yakovlev, Sov. Phys. Solid State **25**, 1733 (1983).
24. E. F. Gross and H. A. Karryev, Dokl. Akad. Nauk SSSR **84**, 471 (1952).
25. E. L. Ivchenko, Phys. Status Solidi A **164**, 487 (1997).
26. E. L. Ivchenko and A. Yu. Kaminskii, Phys. Solid State **37**, 768 (1995).
27. D. R. Yakovlev, A. V. Platonov, E. L. Ivchenko, V. P. Kochereshko, C. Sas, W. Ossau, L. Hansen, A. Waag, G. Landwehr, and L. W. Molenkamp, Phys. Rev. Lett. **88**, 257401 (2002).
28. E. Blackwood, M. J. Snelling, R. T. Barley, S. R. Andrews, and C. T. B. Foxon, Phys. Rev. B **50**, 14246 (1994).
29. J. M. Trombetta, T. A. Kennedy, W. Tseng, and D. Gammon, Phys. Rev. B **43**, 2458 (1991).
30. P. G. Baranov, I. V. Mashkov, N. G. Romanov, K. Gordon, F. Lavallar, and R. Planel', JETP Lett. **60**, 445 (1994).
31. N. G. Romanov, P. G. Baranov, I. V. Mashkov, P. Lavallard, and R. Planel, Solid-State Electron. **37**, 911 (1994).
32. P. G. Baranov, N. G. Romanov, I. V. Mashkov, G. Khitrova, Kh. M. Gibbs, and O. Lungnes, Phys. Solid State **37**, 1648 (1995).
33. S. Yu. Verbin, S. A. Permogorov, and A. N. Reznitskii, Sov. Phys. Solid State **25**, 195 (1983).
34. A. Reznitsky, S. Verbin, S. Permogorov, A. Kornievsky, L. Tenishev, A. Yu. Kaminskii, H. Gerlach, M. Grün, M. Hetterich, and C. Klingshirn, in *Proceedings of the 23rd International Conference on Physics of Semiconductors, Berlin, Germany, 1996*.
35. A. N. Starukhin, D. K. Nelson, and B. S. Razbirin, Phys. Rev. B **65**, 193204 (2002).
36. A. N. Starukhin, D. K. Nelson, B. S. Razbirin, D. L. Fedorov, and D. K. Syunyaev, Phys. Solid State **57**, 1937 (2015).
37. L. Biadala, B. Siebers, R. Gomes, Z. Hens, D. R. Yakovlev, and M. Bayer, J. Phys. Chem. C **118**, 22309 (2014).
38. M. Chamarro, C. Gourdon, and P. Lavallard, J. Lumin. **70**, 222 (1996).
39. L. Langof, L. Fradkin, E. Ehrenfreund, E. Lifshitz, O.I. Micic, and A. J. Nozik, Chem. Phys. **297**, 93 (2004).
40. S. Lee, M. Dobrowolska, and J. K. Furdyna, J. Cryst. Growth **275**, e2301 (2005).
41. L. Turyanska, J. H. Blokland, U. Elfurawi, O. Makarovsky, P. C. M. Christianen, and A. Patanè, Phys. Rev. B **82**, 193302 (2010).
42. Feng Liu, A. V. Rodina, D. R. Yakovlev, A. Greilich, A. A. Golovatenko, A. S. Susha, A. L. Rogach, Yu. G. Kusrayev, and M. Bayer, Phys. Rev. B **89**, 115306 (2014).
43. Y. Masumoto, Ken Toshiyuki, T. Suzuki, and M. Ikezawa, Phys. Rev. B **77**, 115331 (2008).
44. G. E. Pikus and E. L. Ivchenko, in *Excitons*, Ed. by E. I. Rashba and M. D. Sturdge (North-Holland, Amsterdam, 1982), Chap. 6.
45. D. Andronikov, V. Kochereshko, A. Platonov, T. Barrick, S. A. Crooker, and G. Karczewski, Phys. Rev. B **72**, 165339 (2005).

46. K. Kheng, R. T. Cox, Y. Merle d'Aubigne, F. Bassani, K. Saminadayar, and S. Tatarenko, Phys. Rev. Lett. **71**, 1752 (1993).
47. D. R. Yakovlev, J. Puls, G. V. Mikhailov, G. V. Astakhov, V. P. Kochereshko, W. Ossau, J. Nürnberger, W. Faschinger, F. Henneberger, and G. Landwehr, Phys. Status Solidi A **178**, 501 (2000).
48. C. R. L. P. N. Jeukens, P. C. M. Cristianen, J. C. Maan, D. R. Yakovlev, W. Ossau, V. P. Kochereshko, T. Wojtowicz, G. Karczewski, and J. Kossut, Phys. Rev. B **66**, 235318 (2002).
49. J. G. Tischler, A. S. Bracker, D. Gammon, and D. Park, Phys. Rev. B **66**, 081310 (2002).
50. D. A. Andronikov, M. Fehr, V. P. Kochereshko, S. A. Crooker, and G. Karczewski, Phys. Solid State **49**, 1567 (2007).
51. M. Lorenzon, S. Christodoulou, G. Vaccaro, J. Pedrini, F. Meinardi, I. Moreels, and S. Brovelli, Nat. Commun. **6**, 6434 (2015).
52. G. V. Astakhov, D. R. Yakovlev, V. V. Rudenkov, P. C. M. Christianen, T. Barrick, S. A. Crooker, A. B. Dzyubenko, W. Ossau, J. C. Maan, G. Karczewski, and T. Wojtowicz, Phys. Rev. B **71**, 201312 (2005).
53. J. Puls, S. Sadofev, and F. Henneberger, Phys. Rev. B **85**, 041307 (2012).
54. K. Kośmider, J. W. González, and J. Fernández-Rossier, Phys. Rev. B **88**, 245436 (2013).
55. A. Kormányos, G. Burkard, M. Gmitra, J. Fabian, V. Zólyomi, N. D. Drummond, and V. Fal'ko, 2D Mater. **2**, 022001 (2015).
56. G. Wang, L. Bouet, M. M. Glazov, T. Amand, E. L. Ivchenko, E. Palleau, X. Marie, and B. Urbaszek, 2D Mater. **2**, 0340022 (2015).
57. E. Courtade, M. Semina, M. Manca, M. M. Glazov, C. Robert, F. Cadiz, G. Wang, T. Taniguchi, K. Watanabe, M. Pierre, W. Escoffier, E. L. Ivchenko, P. Renucci, X. Marie, T. Amand, and B. Urbaszek, Phys. Rev. B **96**, 085302 (2017).
58. I. A. Akimov, T. Godde, K. V. Kavokin, D. R. Yakovlev, I. I. Reshina, I. V. Sedova, S. V. Sorokin, S. V. Ivanov, Yu. G. Kusrayev, and M. Bayer, Phys. Rev. B **95**, 155303 (2017).
59. K. V. Kavokin, I. A. Merkulov, D. R. Yakovlev, W. Ossau, and G. Landwehr, Phys. Rev. B **60** 16499 (1999).
60. A. V. Kudinov, Yu. G. Kusraev, and V. N. Yakimovich, Phys. Solid State **37**, 359 (1995).
61. V. B. Timofeev, Semiconductors **46**, 843 (2012).
62. A. V. Larionov, V. D. Kulakovskii, S. Höfling, C. Schneider, L. Worschech, and A. Forchel, Phys. Rev. Lett. **105**, 256401 (2010).
63. C. Sturm, D. Solnyshkov, O. Krebs, A. Lemaître, I. Sagnes, E. Galopin, A. Amo, G. Malpuech, and J. Bloch, Phys. Rev. B **91**, 155130 (2015).
64. A. S. Brichkin, S. I. Novikov, A. V. Chernenko, C. Schneider and S. Hoefling, J. Exp. Theor. Phys. **124**, 751 (2017).
65. V. P. Kochereshko, D. V. Avdoshina, P. Savvidis, S. I. Tsintzos, Z. Hatzopoulos, A. V. Kavokin, L. Besombes, and H. Mariette, Semiconductors **50**, 1506 (2016).

Translated by S. Efimov